Oxygen Evolution Reaction

International Edition: DOI: 10.1002/anie.201701998
German Edition: DOI: 10.1002/ange.201701998

Phase-Selective Syntheses of Cobalt Telluride Nanofleeces for Efficient Oxygen Evolution Catalysts

Qiang Gao[+], Chuan-Qi Huang[+], Yi-Ming Ju, Min-Rui Gao, Jian-Wei Liu, Duo An, Chun-Hua Cui, Ya-Rong Zheng, Wei-Xue Li, and Shu-Hong Yu**

Abstract: *Cobalt-based nanomaterials have been intensively explored as promising noble-metal-free oxygen evolution reaction (OER) electrocatalysts. Herein, we report phase-selective syntheses of novel hierarchical $CoTe_2$ and CoTe nanofleeces for efficient OER catalysts. The $CoTe_2$ nanofleeces exhibited excellent electrocatalytic activity and stablity for OER in alkaline media. The $CoTe_2$ catalyst exhibited superior OER activity compared to the CoTe catalyst, which is comparable to the state-of-the-art RuO_2 catalyst. Density functional theory calculations showed that the binding strength and lateral interaction of the reaction intermediates on $CoTe_2$ and CoTe are essential for determining the overpotential required under different conditions. This study provides valuable insights for the rational design of noble-metal-free OER catalysts with high performance and low cost by use of Co-based chalcogenides.*

The oxygen evolution reaction (OER) plays a significant role in many electrochemical processes, such as water splitting and solar fuel synthesis.[1] Design and synthesis of active, stable, and low-cost catalytic materials for water splitting is pivotal to the development of sustainable energy resources for powering fuel cells.[2] In practice, however, large-scale electrochemical production of hydrogen from water splitting is greatly constrained by two fundamental limitations, namely the high overpotentials of the OER, and the lack of stability of electrode materials.[3] Currently, the most widely used catalysts for OER in electrolysis cells are ruthenium (Ru) and iridium (Ir) oxides, although these elements are among the rarest elements on earth.[4] Therefore, there is an urgent demand for alternative catalysts which are not only suitable for large-scale adoption but also retain high efficiency.

In the last few decades, cobalt (Co)-based OER catalysts have been developed for potential applications of water oxidation in alkaline environments, including nanostructured Co_3O_4[5] and related hybrids,[6] Co_2O_3 nanoparticles,[7] amorphous cobalt–phosphate-based materials (Co-P_i),[8] Co-P_i/α-Fe_2O_3 composites,[9] and Co-OEC (oxygen evolving complex).[10] Besides advantages, such as high-abundancy of the metal, low cost, and high synthetic yields, these Co-based materials can generate O_2 under mild conditions and modest overpotentials. Previous efforts have demonstrated that $CoSe_2$ nanobelts and $CoSe_2/Mn_3O_4$ composites are promising OER catalysts in alkaline media.[11] Herein, we show new applications of Te, because compared to O, S and Se chalcogenides, Te exhibits more metallic character, which is a favorable property for electrocatalysts owing to better electronic conductivity.[12]

Although many metal tellurides have been synthesized, research into cobalt telluride hierarchical structures and their applications are still rare.[13] Among various fabrication methods, Te-nanowire-directed synthesis is emerging as one of the most popular strategies for the fabrication of 1D telluride nanostructures,[14] because ultrathin nanowires are desirable templates for the fabrication of 1D nanostructures.[15] Herein, we report a facile chemical transformation process for phase-selective syntheses of uniform hierarchical $CoTe_2$ and CoTe nanofleeces using ultrathin Te nanowires as templates, which shows highly efficient OER performances. The $CoTe_2$ catalyst exhibited superior OER activity over the CoTe catalyst and rivaled the state-of-the-art RuO_2 catalyst in basic media. Furthermore, such hierarchical $CoTe_2$ nanofleeces also perform stably in 0.1M KOH electrolyte. Density functional theory (DFT) calculations showed that the distinct binding strength and lateral interaction of the reaction intermediates on $CoTe_2$ and CoTe is essential for the relative order of their overpotentials and property variations under different conditions.

Firstly, ultrathin Te nanowires (Figure S1, Supporting Information) were synthesized by the modified method described previously.[16] The hierarchical $CoTe_2$ nanofleeces were typically synthesized through a polyol reduction

[*] Dr. Q. Gao,[+] Y. M. Ju, Dr. M. R. Gao, Dr. J. W. Liu, D. An, Dr. C. H. Cui, Dr. Y. R. Zheng, Prof. Dr. S. H. Yu
Department of Chemistry, Division of Nanomaterials and Chemistry, Hefei National Laboratory for Physical Sciences at Microscale, Collaborative Innovation Center of Suzhou Nano Science and Technology, Center for Excellence in Nanoscience, Hefei Science Centre of CAS,
University of Science and Technology of China
Hefei, Anhui 230026 (P.R. China)
E-mail: shyu@ustc.edu.cn
C. Q. Huang,[+] Prof. Dr. W. X. Li
State Key Laboratory of Catalysis, Dalian Institute of Chemical Physics, University of Chinese Academy of Sciences,
Chinese Academic of Sciences
Dalian 116023 (P.R. China)
and
Department of Chemical Physics, Hefei National Laboratory for Physical Sciences at Microscale, iChEM (Collaborative Innovation Center of Chemistry for Energy Materials), Center for Excellence in Nanoscience,
University of Science and Technology of China
Hefei, Anhui 230026 (P.R. China)
E-mail: wxli70@ustc.edu.cn
[+] These authors contributed equally to this work.
Supporting information and the ORCID identification number(s) for the author(s) of this article can be found under: https://doi.org/10.1002/anie.201701998.

approach using the ultrathin Te nanowires as templates. The X-ray diffraction (XRD) patterns (Figure S2) of the samples obtained at 200 °C and 220 °C can be indexed to orthorhombic $CoTe_2$ (JCPDS 11-0553) and hexagonal CoTe (JCPDS 34-0420), respectively. The Co:Te atomic ratio determined by energy-dispersive X-ray spectroscopy (EDS) analysis (Figure S3) agrees well with the XRD result. The X-ray photoelectron spectroscopy (XPS) binding energy data in Figure S4a reveal that the Co atoms in $CoTe_2$ and CoTe both correspond to Co^{2+} cations.[17] Furthermore, synchrotron X-ray absorption spectroscopy (XAS) analysis also confirmed the Co^{2+} oxidation state for both $CoTe_2$ and CoTe(Figure S4b).

The morphologies and sizes of the products were studied by field-emission scanning electron microscopy (FESEM) and transmission scanning electron microscopy. Figure 1a shows a typical SEM image of the hierarchical $CoTe_2$ structures with a mean diameter of about 200 nm and length up to several micrometers. The SEM image indicates that a large amount of small nanofleeces align perpendicularly to the growth axis, forming remarkable 1D hierarchical nanostructures. The representative SEM image of as-prepared products clearly reveals that the small nanofleeces have small diameters of approximately 10 nm, and lengths of tens to hundreds of nanometers. Figure 1b shows a typical HRTEM image of a single $CoTe_2$ nanofleece, revealing that the $CoTe_2$ nanofleeces are structurally uniform with interlayer spacing of about 2.71 Å, which corresponds to the (120) lattice plane of the orthorhombic $CoTe_2$. The elemental mappings (Figure 1c) indicate that Co and Te elements are uniformly distributed in the product. Figure 1d shows a typical SEM image of CoTe nanofleeces, which have a similar hierarchical structure to the $CoTe_2$ nanofleeces. A typical HRTEM image (Figure 1e) of a single CoTe nanofleece reveals that the CoTe hierarchical structures are structurally uniform with interlayer spacing of about 2.86 Å, which corresponds to the (101) lattice plane of the hexagonal CoTe. Moreover, the N_2 adsorption-desorption isotherms of the product (Figure S5) reveal that the hierarchical $CoTe_2$ and CoTe nanofleeces have BET surface areas of 97 and 75 $m^2 g^{-1}$, respectively, which are fairly high for transition-metal–chalcogenide materials. Such a high surface area is attributed to the tiny branched nanofleeces with average diameters of about 10 nm.

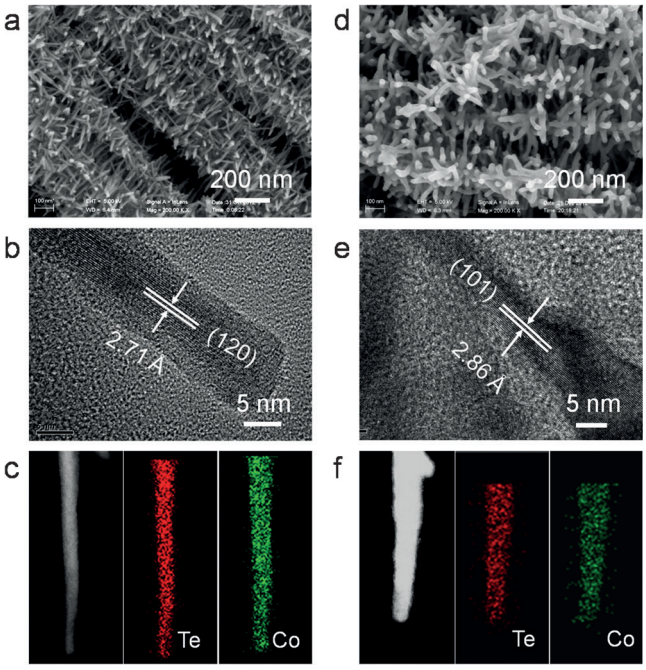

Figure 1. SEM images of hierarchical $CoTe_2$ (a) and CoTe (d) nanostructures. HRTEM image of single $CoTe_2$ (b) and CoTe (e) nanofleeces. c,f) HAADF-STEM characterization of single nanofleeces, and the corresponding elemental mappings of Te (red) and Co (green).

To understand the formation mechanism of hierarchical $CoTe_2$ nanofleeces, the growth process was carefully tracked by time-dependent experiments. We used XRD to analyze the phase evolution of this reaction (Figure S6). After maintaining the solution at 110 °C for 1 h, all of the XRD peaks could be indexed to the hexagonal phase of Te. When the reaction temperature was increased to 200 °C for 15 min, trace peaks of $CoTe_2$ appeared in the XRD pattern, which indicated that $CoTe_2$ began to form. Upon prolonging the reaction time to 30 min, the product consisted predominantly of $CoTe_2$, although the hexagonal phase of Te was also present. No hexagonal Te diffraction peaks were observed when the reaction time was increased to 1 h, which indicated that the Te component was completely transformed into $CoTe_2$.

The samples taken from the synthesis mixtures at different time intervals were then analyzed by SEM to capture the morphology evolution process (Figure 2). Figure 2a shows a schematic illustration of the proposed growth mechanism for hierarchical $CoTe_2$ nanostructures. In order to evaporate the trace amount of water, we first heated the solution at 110 °C for 1 h. During this process, the diameter of the nanowires grew from 7 nm to approximately 30 nm, and the surface of the nanowire became much rougher (Figure S7). When the temperature was raised to 200 °C, numerous growths appeared on the surface of the nanowires. As time progressed, further material grew out of the nanowires, forming long nanofleeces, eventually covering the entire nanowire surface after a 1 h reaction time. As the reaction proceeded to 2 h, the nanofleeces continued to grow, and the average diameter reached about 20 nm. We have conducted a series of experiments to optimize the conditions for the syntheses of high-quality hierarchical $CoTe_2$ nanostructures. In our experiments, we found that the ratio of oleylamine:oleic acid (OAm:OA), the amount of $Co(acac)_2$, the reaction temperature, and reaction time play important roles in the formation of uniform hierarchical $CoTe_2$ nanostructures (Figure S8–S11).

To appraise the catalytic properties of the new hierarchical $CoTe_2$ nanostructures for electrochemical oxidation of water to oxygen, films of hierarchical $CoTe_2$ nanostructures were prepared on glassy carbon electrodes for cyclic voltammetry (CV) in O_2-saturated 0.1M KOH. Similar measurements for hierarchical CoTe nanostructures, Pt/C (20 wt%), and a commercial RuO_2 reference, were also performed for comparison. Figure 3a shows their linear sweeps in an anodic direction, from which we can see that the hierarchical $CoTe_2$ nanostructures exhibit greater current densities as compared

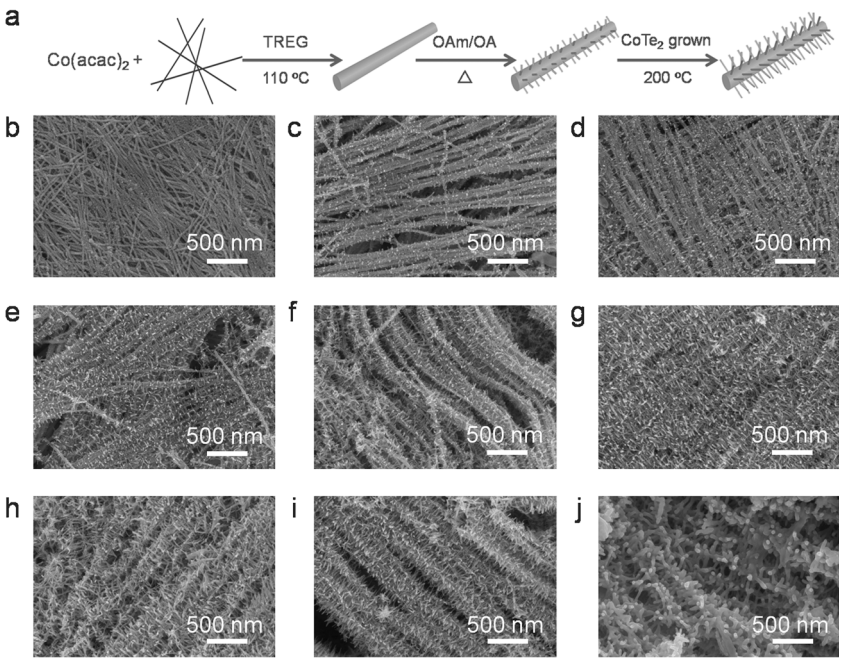

Figure 2. a) Schematic illustration of the proposed growth mechanism for hierarchical $CoTe_2$ nanostructures, TREG = triethylene glycol); b) SEM image of the product obtained at 110 °C for 60 min; SEM images of the products obtained at 200 °C for c) 0; d) 5; e) 10; f) 15; g) 20; h) 30; i) 60; and j) 120 min.

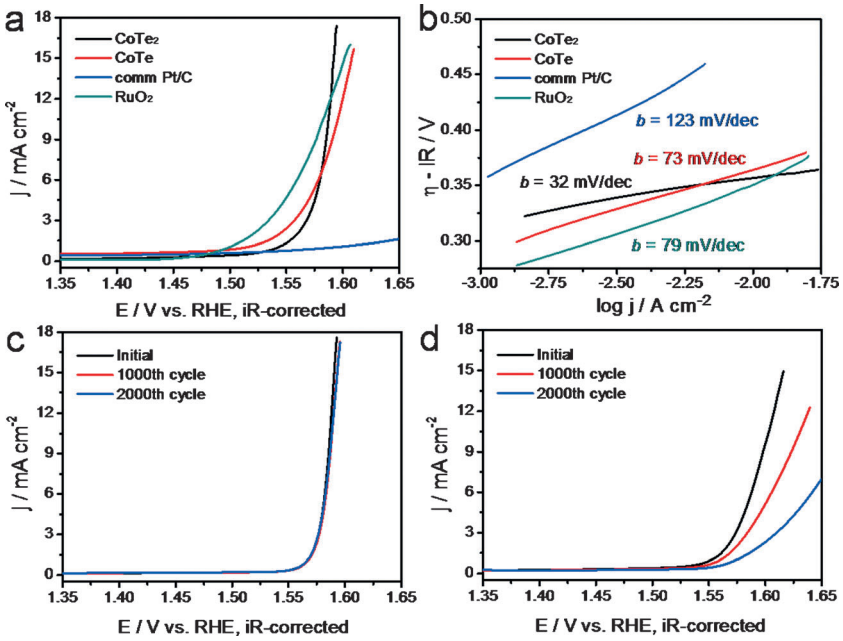

Figure 3. a) Polarization curves for OER of several catalysts as indicated. b) Tafel plot (overpotential versus log current) derived from (a). c, d) OER polarization curves of hierarchical $CoTe_2$ (c) and CoTe (d) nanofleeces before and after different cycles of accelerated stability tests.

to hierarchical CoTe nanostructures, Pt/C, and RuO_2. The current density of 10 mA cm^{-2} can be achieved at a small overpotential of approximately 0.357 V for our catalyst, which is better than the best reported Co_3O_4/graphene catalyst with a similar loading (0.25 mg cm^{-2}).[6] Note that the overpotential of current density at 10 mA cm^{-2} of the $CoTe_2$ catalyst is comparable to, or smaller than, those of the well-studied Co-based OER catalysts in the literature (Table S1). Figure 3b shows that the Tafel slope of the hierarchical $CoTe_2$ nanostructures is approximately 32 mV dec^{-1}, which is smaller than that of RuO_2, hierarchical CoTe nanostructures, and previously reported Co-based OER catalysts such as $CoSe_2/Mn_3O_4$ composites,[11a] Co_3O_4[5] and Co_3O_4/graphene hybrids[6] at similar loading, and comparable to the best known OER catalysts in basic media.[18] We calculated a TOF (turnover frequency) of 0.20 s^{-1} associated with $CoTe_2$ nanostructures at an overpotential of 350 mV in 0.1 M KOH, which was higher than the 0.12 s^{-1} of CoTe nanostructures, and comparable to 0.22 s^{-1} of RuO_2.

In addition, the hierarchical $CoTe_2$-nanostructured catalyst also exhibited high stability for OER. Figure 3c shows that after 2000 potential cycles, the $CoTe_2$ nanostructures afforded nearly unchanged *J–V* curves, only with negligible decreases to the anodic current, while the anodic current decreased by about 80% and 70% for the hierarchical CoTe nanostructures (Figure 3d) and the state-of-the-art RuO_2 (Figure S12) at 1.60 V versus RHE (reversible hydrogen electrode), respectively. We performed XRD and XPS measurements after 2000 potential cycles (Figure S13, S14), which showed that no obvious phase and valence changes were observed after long-term electrolysis. As shown in Figure S13c,d, the original hierarchical nanostructure of $CoTe_2$ was retained after 2000 potential cycles of electrolysis, while the morphology of CoTe was destroyed, which explains the different stabilities of $CoTe_2$ and CoTe catalysts. The excellent stability of the $CoTe_2$ system can be evidenced further from the chronoamperometric measurements. As shown in Figure S15, at a current density of 10 mA cm^{-2}, the overpotential produced in the $CoTe_2$ catalyst exhibited no measurable increase over 24 h of continuous operation. This extraordinary durability shows promise for practical applications of the catalysts over the long term.

We then studied the OER activities of the products obtained at different time intervals (Figure S16a). The low OER activities of the products obtained at 15 min and 30 min are attributed to the presence of impurities and the poor crystallinity of remnant Te nanowires, while the low OER

activities of the products obtained at 2 h could be the result of low surface areas. We also studied the OER activities of the products obtained at different temperatures (Figure S16b). The low OER activities of the products obtained at 180 °C are also attributed to impurities and poor crystallinity of remnant Te nanowires, while the low OER activities of the materials obtained at 250 °C are attributed to the particular phase of CoTe its even lower surface area.

To rationalize the superior electrochemical performance of $CoTe_2$ and dependence on the phase, we propose that high surface area, electrical conductivity, and activities between the reaction intermediates and $CoTe_2$ or CoTe, are essential. Firstly, the hierarchical structure of $CoTe_2$ nanofleeces offers large surface areas, which increases contact between the electrolytes and electrode materials, thus enhancing the electrocatalytic activities of the electrodes. This can be justified by the larger BET area of 97 and 75 $m^2 g^{-1}$ for $CoTe_2$ and CoTe, respectively (Figure S5). To gain more insights into the electrochemically active surface area of materials, the capacitance of the corresponding double-layer of $CoTe_2$ and CoTe nanostructures were measured. As shown in Figure S17, the capacitance of $CoTe_2$ electrode is 0.357 mF cm^{-2}, while the capacitance of CoTe electrode is 0.266 mF cm^{-2}. Therefore, the $CoTe_2$ catalysts have a more electroactive surface than that of CoTe, which corroborates its enhanced reactivity. Secondly, the kinetics of electrode reactions for $CoTe_2$ and CoTe nanostructures were probed by electrochemical impedance spectroscopy (EIS) techniques (Figure S18). The smaller R_{ct} value found for $CoTe_2$ electrodes, compared with that of CoTe, suggests a higher electrical conductivity for $CoTe_2$.

DFT investigations (see Supporting Information for details) of the two dominant facets, CoTe(101) and $CoTe_2$-(120) (Figure S19 and S20), showed that $CoTe_2$ and CoTe bind differently with the reaction intermediates involved in OER.[19] The standard reaction free energy profiles ΔG (Figure 4), taking into account the electrochemical condition,[19b,20] shows that the third step is potentially the limiting step (see Table S3 for details), which is consistent with previous calculations on metals or metal oxides in acidic conditions.[19c,20,21] At a lower coverage of 0.5 monolayer (with respect to surface five-fold Co atoms), the corresponding overpotential of $CoTe_2$ is 1.01 V, which is larger than that of 0.92 V for CoTe. This explains why the observed η of $CoTe_2$ is larger than that of CoTe at low current (Figure 3a). With an increase of the applied external potential (and the current), anionic OH^- tends to accumulate at the anode, forming adsorbed OH*, O*, and OOH* species (* indicating an adsorption site), and increasing the surface coverage. By calculating the ΔG profile in the presence of 0.5 monolayer pre-adsorbed OH*/O*/OOH* (see Figure S21, S22 and Table S2, S3), it is not surprising that the differential binding strength for all intermediates involved are weakened on both surfaces because of increased lateral repulsion. Interestingly, the extents of destabilization for the intermediates considered on two surfaces are different, especially for O* and OOH*. Accordingly, the order of the overpotential between $CoTe_2$-(120) and CoTe(101) is reversed with the pre-adsorbed species. This can be seen in the free-energy profile with pre-adsorbed 0.5 monolayer O* plotted in Figure 4c and 4d. This shows that the different lateral interactions between the reaction intermediates at higher coverage have a high impact on the overpotential. The computational result rationalizes the trend variation of the electrocatalytic activity of $CoTe_2$-(120) and CoTe(101) under different conditions.

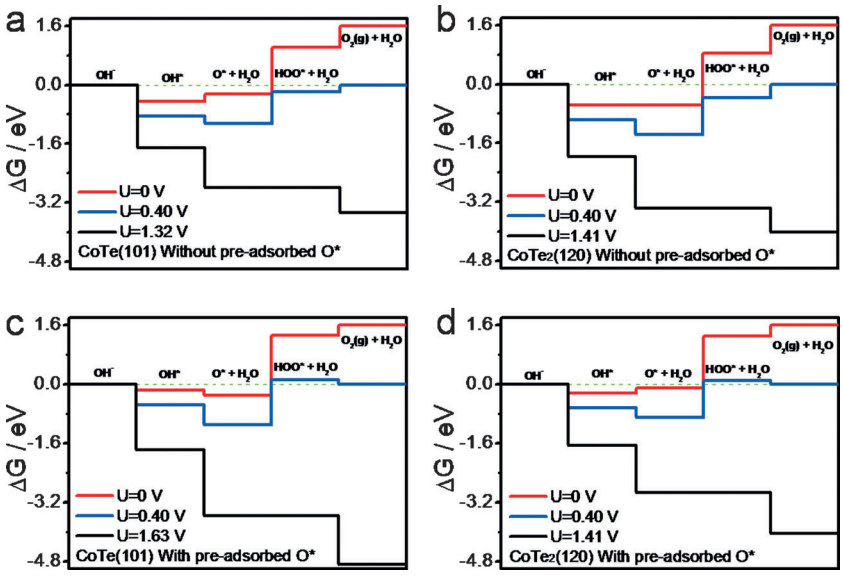

Figure 4. Standard free-energy diagram for OER at zero potential, equilibrium potential and theoretical onset external potential. a, b): for CoTe(101) and $CoTe_2$(120) without pre-adsorbed O*; c, d): for CoTe(101) and $CoTe_2$(120) with pre-adsorbed O* (0.5 monolayer).

In summary, we have demonstrated a facile chemical transformation process for phase-selective syntheses of novel hierarchical $CoTe_2$ and CoTe nanofleeces using ultrathin Te nanowires as templates. This $CoTe_2$ catalyst exhibited excellent OER activity and stability in alkaline media. The high surface area and electrical conductivity of $CoTe_2$ and CoTe nanostructures played an essential role in their superior electrocatalytic performances. DFT calculations showed that the binding strengths and lateral interactions of the reaction intermediates involved on $CoTe_2$ and CoTe in OER are essential for determining the overpotential required under different conditions. This study describes the significant potential for designing high-performance and low-cost OER catalysts from metal tellurides, which are desirable for energy conversion technologies.

Acknowledgements

We acknowledge the funding support from the National Natural Science Foundation of China (Grants 21521001,

21431006, 21225315, 21321002, 91645202), the National Basic Research Program of China (Grants 2014CB931800, 2013CB834603), the Users with Excellence and Scientific Research Grant of Hefei Science Center of CAS (2015HSC-UE007), the Key Research Program of Frontier Sciences, CAS (Grant QYZDJ-SSW-SLH036), and the Chinese Academy of Sciences (Grants KGZD-EW-T05, XDA090301001), and the Fundamental Research Funds for the Central Universities (WK2060190045).

Conflict of interest

The authors declare no conflict of interest.

Keywords: cobalt · electrocatalyst · hierarchical structure · oxygen evolution reaction · tellurium

[1] a) Q. Yin, J. M. Tan, C. Besson, Y. V. Geletii, D. G. Musaev, A. E. Kuznetsov, Z. Luo, K. I. Hardcastle, C. L. Hill, *Science* **2010**, *328*, 342; b) M. W. Kanan, D. G. Nocera, *Science* **2008**, *321*, 1072.

[2] M.-R. Gao, J.-X. Liang, Y.-R. Zheng, Y.-F. Xu, J. Jiang, Q. Gao, J. Li, S.-H. Yu, *Nat. Commun.* **2015**, *6*, 5982.

[3] R. Subbaraman, D. Tripkovic, K. C. Chang, D. Strmcnik, A. P. Paulikas, P. Hirunsit, M. Chan, J. Greeley, V. Stamenkovic, N. M. Markovic, *Nat. Mater.* **2012**, *11*, 550.

[4] a) F. A. Frame, T. K. Townsend, R. L. Chamousis, E. M. Sabio, T. Dittrich, N. D. Browning, F. E. Osterloh, *J. Am. Chem. Soc.* **2011**, *133*, 7264; b) V. Petrykin, K. Macounova, O. A. Shlyakhtin, P. Krtil, *Angew. Chem. Int. Ed.* **2010**, *49*, 4813; *Angew. Chem.* **2010**, *122*, 4923.

[5] A. J. Esswein, M. J. McMurdo, P. N. Ross, A. T. Bell, T. D. Tilley, *J. Phys. Chem. C* **2009**, *113*, 15068.

[6] Y. Liang, Y. Li, H. Wang, J. Zhou, J. Wang, T. Regier, H. Dai, *Nat. Mater.* **2011**, *10*, 780.

[7] T.-L. Wee, B. D. Sherman, D. Gust, A. L. Moore, T. A. Moore, Y. Liu, J. C. Scaiano, *J. Am. Chem. Soc.* **2011**, *133*, 16742.

[8] a) Y. Surendranath, M. Dinca, D. G. Nocera, *J. Am. Chem. Soc.* **2009**, *131*, 2615; b) D. A. Lutterman, Y. Surendranath, D. G. Nocera, *J. Am. Chem. Soc.* **2009**, *131*, 3838.

[9] a) D. K. Zhong, D. R. Gamelin, *J. Am. Chem. Soc.* **2010**, *132*, 4202; b) D. K. Zhong, J. Sun, H. Inumaru, D. R. Gamelin, *J. Am. Chem. Soc.* **2009**, *131*, 6086.

[10] S. Y. Reece, J. A. Hamel, K. Sung, T. D. Jarvi, A. J. Esswein, J. J. H. Pijpers, D. G. Nocera, *Science* **2011**, *334*, 645.

[11] a) M. R. Gao, Y. F. Xu, J. Jiang, Y. R. Zheng, S. H. Yu, *J. Am. Chem. Soc.* **2012**, *134*, 2930; b) M. R. Gao, W. T. Yao, H. B. Yao, S. H. Yu, *J. Am. Chem. Soc.* **2009**, *131*, 7486.

[12] G. Wu, G. F. Cui, D. Y. Li, P. K. Shen, N. Li, *J. Mater. Chem.* **2009**, *19*, 6581.

[13] a) I. G. McKendry, A. C. Thenuwara, J. Sun, H. Peng, J. P. Perdew, D. R. Strongin, M. J. Zdilla, *ACS Catal.* **2016**, *6*, 7393; b) S. A. Patil, E.-K. Kim, N. K. Shrestha, J. Chang, J. K. Lee, S.-H. Han, *ACS Appl. Mater. Interfaces* **2015**, *7*, 25914; c) R. Shi, X. Liu, Y. Shi, R. Ma, B. Jia, H. Zhang, G. Qiu, *J. Mater. Chem.* **2010**, *20*, 7634; d) H. Fan, Y. Zhang, M. Zhang, X. Wang, Y. Qian, *Cryst. Growth Des.* **2008**, *8*, 2838; e) Q. Peng, Y. Dong, Y. Li, *Inorg. Chem.* **2003**, *42*, 2174; f) Y. Xie, B. Li, H. Su, X. Liu, Y. Qian, *Nanostruct. Mater.* **1999**, *11*, 539.

[14] a) H. W. Liang, S. Liu, Q. S. Wu, S. H. Yu, *Inorg. Chem.* **2009**, *48*, 4927; b) J. Li, X. Tang, L. Song, Y. Zhu, Y. Qian, *J. Cryst. Growth* **2009**, *311*, 4467; c) P. Zuo, S. Zhang, B. Jin, Y. Tian, J. Yang, *J. Phys. Chem. C* **2008**, *112*, 14825.

[15] a) H. W. Liang, J. W. Liu, H. S. Qian, S. H. Yu, *Acc. Chem. Res.* **2013**, *46*, 1450; b) R. L. S. Tan, W. H. Chong, Y. Feng, X. Song, C. L. Tham, J. Wei, M. Lin, H. Chen, *J. Am. Chem. Soc.* **2016**, *138*, 10770; c) J. He, Y. Wang, Y. Feng, X. Qi, Z. Zeng, Q. Liu, W. S. Teo, C. L. Gan, H. Zhang, H. Chen, *ACS Nano* **2013**, *7*, 2733.

[16] H. S. Qian, S. H. Yu, J. Y. Gong, L. B. Luo, L. F. Fei, *Langmuir* **2006**, *22*, 3830.

[17] NIST X-ray Photoelectron Spectroscopy Database. http://srdata.nist.gov/xps/Default.aspx.

[18] a) L. Trotochaud, J. K. Ranney, K. N. Williams, S. W. Boettcher, *J. Am. Chem. Soc.* **2012**, *134*, 17253; b) J. Suntivich, K. J. May, H. A. Gasteiger, J. B. Goodenough, Y. Shao-Horn, *Science* **2011**, *334*, 1383.

[19] a) A. Vojvodic, J. K. Norskov, *Science* **2011**, *334*, 1355; b) H. Y. Su, Y. Gorlin, I. C. Man, F. Calle-Vallejo, J. K. Norskov, T. F. Jaramillo, J. Rossmeisl, *Phys. Chem. Chem. Phys.* **2012**, *14*, 14010; c) M. Bajdich, M. Garcia-Mota, A. Vojvodic, J. K. Norskov, A. T. Bell, *J. Am. Chem. Soc.* **2013**, *135*, 13521.

[20] J. Rossmeisl, A. Logadottir, J. K. Nørskov, *Chem. Phys.* **2005**, *319*, 178.

[21] A. Valdés, J. Brillet, M. Grätzel, H. Gudmundsdottir, H. A. Hansen, H. Jónsson, P. Klüpfel, G. J. Kroes, F. Le Formal, I. C. Man, R. S. Martins, J. K. Nørskov, J. Rossmeisl, K. Sivula, A. Vojvodic, M. Zäch, *Phys. Chem. Chem. Phys.* **2012**, *14*, 49.

Manuscript received: February 23, 2017
Revised manuscript received: April 29, 2017
Accepted manuscript online: May 3, 2017
Version of record online: ■■ ■■, ■■■■

Communications

Oxygen Evolution Reaction

Q. Gao, C. Q. Huang, Y. M. Ju, M. R. Gao, J. W. Liu, D. An, C. H. Cui, Y. R. Zheng, W. X. Li,* S. H. Yu* _____ ■■■■–■■■■

Phase-Selective Syntheses of Cobalt Telluride Nanofleeces for Efficient Oxygen Evolution Catalysts

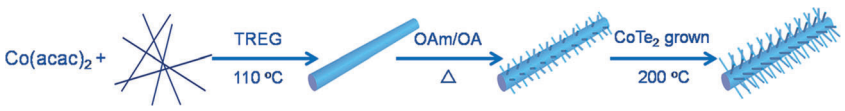

Fleeced: Hierarchical $CoTe_2$ nanofleeces were synthesized by using ultrathin Te nanowires as templates. They exhibited excellent electrocatalytic activity and stablity for the oxygen evolution reaction (OER) in alkaline media. The $CoTe_2$ catalyst exhibited superior OER activity to the CoTe catalyst and was comparable to the state-of-the-art RuO_2 catalyst.

